Available online at www.sciencedirect.com
ScienceDirect
Journal of Colloid and Interface Science 318 (2008) 238–243
JOURNAL OF Colloid and Interface Science
www.elsevier.com/locate/jcis

Kinetics of gold nanoparticle aggregation: Experiments and modeling

Taehoon Kim [a], Chang-Ha Lee [a], Sang-Woo Joo [b,*], Kangtaek Lee [a,*]

[a] *Department of Chemical Engineering, Yonsei University, Seoul 120-749, Republic of Korea*
[b] *Department of Chemistry, Soongsil University, Seoul 156-743, Republic of Korea*

Received 24 August 2007; accepted 16 October 2007

Available online 19 November 2007

Abstract

We investigate the aggregation kinetics of gold nanoparticles using both experimental techniques (i.e., quasi-elastic light scattering, UV–visible spectroscopy, and transmission electron microscopy) and mathematical modeling (i.e., constant-number Monte Carlo). Aggregation of gold nanoparticles is induced by replacing the surface citrate groups with benzyl mercaptan. We show that the experimental results can be well described by the model in which interparticle interactions are described by the classical DLVO theory. We find that final gold nanoparticle aggregates have a fractal structure with a mass fractal dimension of 2.1–2.2. Aggregation of approximately 11 initial gold nanoparticles appears to be responsible for the initial color change of suspension. This kinetic study can be used to predict the time required for the initial color change of a gold nanoparticle suspension and should provide insights into the design and optimization of colorimetric sensors that utilize aggregation of gold nanoparticles.

Keywords: Gold; Nanoparticle; Aggregation; Kinetics; Fractal structure; Colorimetric sensor

1. Introduction

Gold nanoparticles have attracted much attention due to their uniformity and optical properties since the report by Faraday [1,2]. The introduction of the citrate-reduction method by Turkevich and co-workers enabled quick and easy preparation of gold nanoparticles with sizes on the order of tens of nanometers [3]. Gold nanoparticles find applications in various fields, including chemical, medical, and biological sciences [4–6].

One of the most promising applications of gold nanoparticles is in colorimetric sensors for specific target detection. Aggregation of gold nanoparticles leads to a change in their optical properties (i.e., a red shift in surface plasmons, or a red-to-blue color change as detected by the naked eye), which can be used in the colorimetric detection of target agents [7–9]. The localized surface plasmon resonance of metal nanoparticles that is responsible for the change in optical properties results from collective oscillation of conduction electrons upon interaction with electromagnetic radiation [10,11]. Mirkin and co-workers showed that the change in the localized surface plasmon band should be related to the aggregated size [8]. For practical applications of gold nanoparticles as colorimetric sensors, though, there still remain issues such as the response time control and miniaturization. To resolve these issues, it is essential to understand the kinetics of the aggregation process [12–15]. We have recently investigated the aggregation of gold nanoparticles in real time and analyzed colloidal stability with theoretical interpretations [16]. These results were rationalized by calculating the interparticle interaction energy and the stability ratio of nanoparticle aggregates.

In this paper, we examine the aggregation kinetics of gold nanoparticles using both experiments and mathematical modeling. The colloidal dispersions of gold nanoparticles are induced to aggregate by replacing the surface citrate groups with benzyl mercaptan, which acts as a well-defined, simple, and robust monolayer adsorbate [16]. The stability ratios calculated from classical DLVO theory are used to rationalize the experimental results [17,18], and the constant-number Monte Carlo method [19] is used to model the aggregation kinetics.

* Corresponding authors.
E-mail addresses: sjoo@ssu.ac.kr (S.-W. Joo), ktlee@yonsei.ac.kr (K. Lee).

0021-9797/$ – see front matter
doi:10.1016/j.jcis.2007.10.029

This work is, to the best of our knowledge, the first comprehensive kinetic study of gold nanoparticle aggregation that can be used to predict the time required for the initial color change of a suspension. Since the response time of biological sensors is a crucial factor in the detection of target agents, this work will be useful in the design and optimization of sensors based on gold nanoparticle aggregation.

2. Materials and methods

2.1. Preparation and characterization of gold nanoparticle aggregates

Stable suspensions of gold nanoparticles were prepared by the citrate-reduction method [3]. A 0.01% potassium tetrachloroaurate (III) solution ($KAuCl_4$, Aldrich) in water was brought to boiling with trisodium citrate dihydrate. The sizes of gold nanoparticles in this reductive synthesis were controlled by changing the amount of citrate added. The concentration of trisodium citrate was set to 13.0×10^{-4} M for samples A1–A3 and 5.5×10^{-4} M for samples B1–B3. After stable suspension of gold nanoparticles was formed, we added a concentrated ethanolic solution of benzyl mercaptan in suspension to induce aggregation. The concentration of benzyl mercaptan was set to 5.0×10^{-5} M (samples A1 and B1), 7.5×10^{-5} M (samples A2 and B2), and 10.0×10^{-5} M (A3 and B3).

The diameter and zeta potential of particles were monitored by quasi-elastic light scattering (QELS) and zeta potential measurements (Nano-ZS from Malvern Instrument Co). To monitor the change in the optical properties of gold nanoparticle suspension, UV–visible absorption spectroscopy (Shimadzu UV–1650PC spectrophotometer) was used. Transmission electron microscopy (TEM, JEOL JEM-4010) was also used to observe the morphology of gold nanoparticle aggregates.

2.2. Constant-number Monte Carlo with the DLVO interactions

The constant-number Monte Carlo method developed by Smith and Matsoukas [19] was used to model aggregation of gold nanoparticles. In this method, we start with a simulation box containing 30,000 initial particles. First, a pair of particles (i and j) is randomly picked from the initial particle matrix. To determine whether they aggregate, we pick a random number, r, and calculate the aggregation probability, P_{ij}, which is defined as

$$P_{ij} = \frac{K_{ij}}{K_{ij,\max}}. \tag{1}$$

In Eq. (1), K_{ij} is the aggregation rate between particles i and j, and $K_{ij,\max}$ is the maximum aggregation rate among all particle pairs in the simulation box. If r is smaller than P_{ij}, the two particles are allowed to aggregate. If not, a new particle pair is selected and this step is repeated until two particles aggregate. After each aggregation event, the simulation time is increased and a particle is randomly selected from the simulation box and copied onto the empty array to keep the total number of particles constant.

2.3. Calculation of the aggregation probabilities

To calculate the aggregation probability in the Monte Carlo, the aggregation rate, $K(r, r')$ of particles of radius r and r' is defined as follows [16–18]:

$$K(r, r') = K_{\mathrm{B}}(r, r')/W(r, r'). \tag{2}$$

In Eq. (2), $K_{\mathrm{B}}(r, r')$ and $W(r, r')$ are the Brownian aggregation rate and the stability ratio, respectively. The Brownian aggregation rate can be expressed as [17,18]

$$K_{\mathrm{B}}(r, r') = \frac{2kT}{3\mu}(r + r')\left(\frac{1}{r} + \frac{1}{r'}\right). \tag{3}$$

The stability ratio accounts for the effect of interparticle interaction on the aggregation rate [17,18],

$$W(r, r') = 2\int_0^\infty \frac{\exp[V_{\mathrm{T}}/kT]}{s^2}\,ds. \tag{4}$$

Total interaction potential in Eq. (4), V_{T}, can be expressed as the sum of the electrostatic repulsion (V_{elec}) and the van der Waals attraction (V_{vdw}) according to the classical DLVO theory [17,18]:

$$V_{\mathrm{T}} = V_{\mathrm{elec}} + V_{\mathrm{vdw}}. \tag{5}$$

To calculate the electrostatic repulsion potential, V_{elec}, the following two different forms were used depending on the value of κa [16]:

$$V_{\mathrm{elec}} = 4\pi\varepsilon\psi_0^2\frac{a_1 a_2}{a_1 + a_2}\ln\bigl[1 + \exp(-\kappa x)\bigr] \quad (\text{in the case of } \kappa a > 5), \tag{6}$$

$$V_{\mathrm{elec}} = 4\pi\varepsilon a_1 a_2 Y_1 Y_2\left(\frac{kT}{e}\right)^2\frac{\exp(-\kappa x)}{x + a_1 + a_2} \quad (\text{in the case of } \kappa a < 5). \tag{7}$$

Inverse Debye length (κ) and Y_i are defined as

$$\kappa = \left[\frac{1000e^2 N_{\mathrm{A}}(2I)}{\varepsilon kT}\right]^{1/2}, \tag{8}$$

$$Y_i = \frac{8\tanh(\varepsilon\psi_0/4kT)}{1 + [1 - 2\kappa a_i/(\kappa a_i + 1)^2\tanh^2(\varepsilon\psi_0/4kT)]^{1/2}}. \tag{9}$$

Assuming that gold nanoparticle aggregates were spherical, we used the following form to calculate the van der Waals attraction potential between the two particles:

$$V_{\mathrm{vdw}} = -\frac{A_{\mathrm{H}}}{6}\left[\frac{2a_1 a_2}{R^2 - (a_1 + a_2)^2} + \frac{2a_1 a_2}{R^2 - (a_1 - a_2)^2} + \ln\frac{R^2 - (a_1 + a_2)^2}{R^2 - (a_1 - a_2)^2}\right]. \tag{10}$$

In the above equations, the surface potential was estimated from the zeta potential measurement, and 2.5×10^{-19} J was used for the Hamaker constant (A_{H}) [16].

Table 1
Average diameter and zeta potential of the gold nanoparticle aggregates before and after benzyl mercaptan addition

Sample	Before		After	
	Diameter (nm)	ζ potential (mV)	Diameter (nm)	ζ potential (mV)
A1	14.8	−55.31	38.2	−44.28
A2	14.8	−55.31	61.8	−41.99
A3	14.8	−55.31	78.2	−39.57
B1	38.4	−44.62	204	−35.01
B2	38.4	−44.62	358	−34.37
B3	38.4	−44.62	591	−33.25

3. Results and discussion

Table 1 compares the average diameter and zeta potential of gold nanoparticle aggregates before and after the benzyl mercaptan addition. As the amount of benzyl mercaptan increases, the diameter of the gold nanoparticle aggregates increases, but the value of the zeta potential decreases. This is caused by replacement of the surface citrate ions with mercaptan, which lowers the surface potential of nanoparticles and induces aggregation [16]. Upon the addition of benzyl mercaptan, the zeta potential measurement shows a sudden decrease in value (results not shown), which suggests rapid replacement of citrate ions.

Since the change in the optical property of gold nanoparticles is responsible for their colorimetric sensor applications, we have monitored the change in the optical properties of the gold nanoparticle suspension with UV–vis absorption spectroscopy. Fig. 1 shows the spectral changes of surface plasmon bands resulting from the aggregation of gold nanoparticles. Aggregation causes a decrease in the intensity and a red shift in the characteristic surface plasmon band at ∼520 nm. In addition, the localized surface plasmon band at ∼720 nm appears and it redshifts as the aggregation continues. These spectral changes are accompanied by a corresponding color change in the solution from red to blue. Note that we observe a complementary color for the spectral position of the localized surface plasmon band because we consider only the absorption phenomena in this study. The changes in the visible spectra of all samples after the benzyl mercaptan addition are shown in Fig. 2. TEM images of the two differently colored solutions marked (a) and (b) in Fig. 1 indicate aggregation of the gold nanoparticles.

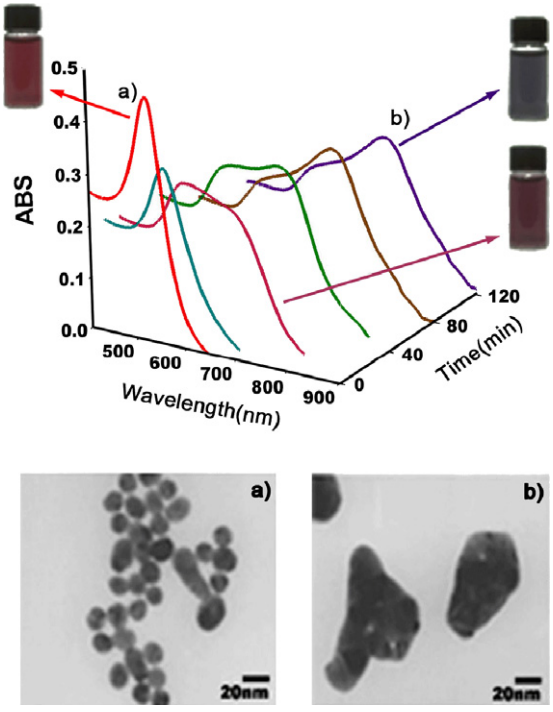

Fig. 1. Color change, appearance of the localized surface plasmon bands in UV–vis absorption spectra, and TEM images of gold nanoparticle aggregates (A3) as a function of time.

Fig. 3 shows the changes in the stability ratio of gold nanoparticle aggregates after benzyl mercaptan addition. Upon the addition of benzyl mercaptan, the citrate ions on the surface are replaced by the benzyl mercaptan. This causes a significant decrease in the stability ratio and aggregation of nanoparticles. As aggregation proceeds, the stability ratio increases again due to the increase in aggregate size, and finally gold nanoparticle aggregates are restabilized. These results are consistent with our previous work [16].

Since mathematical modeling is essential in the quantitative understanding of the process as well as in the design and optimization of sensors based on gold nanoparticle aggregation, we have used the constant-number Monte Carlo method [19] to model the aggregation process. We assume that irreversible aggregation is the only event in gold nanoparticle aggregation. It is also assumed that the replacement of citrate ions with mercaptan is instantaneous, which is supported by the zeta potential measurements. Aggregation of nanoparticles often leads to formation of fractal structures [20], which is also suggested by TEM images in Fig. 1. Thus, we have incorporated the mass fractal dimension into our model. The mass of the fractal object (m) increases with its radius (r) according to [21]

$$m \propto r^{D_f}. \tag{11}$$

Using the above equation, the Brownian aggregation rate, Eq. (3), can be rewritten in terms of particle mass and mass fractal dimension:

$$K_B(m,m') = \frac{2kT}{3\mu}\left(m^{1/D_f} + m'^{1/D_f}\right)\left(m^{-1/D_f} + m'^{-1/D_f}\right). \tag{12}$$

Best fits to average diameter versus time curves have been obtained using D_f as the only fitting parameter.

Fig. 4 shows the evolution of average diameter versus time after benzyl mercaptan addition. It is easily seen that the calculated values are in sufficient agreement with the experimental results in all cases. The mass fractal dimension of gold nanoparticle aggregates is found to be 2.1 (A3 and B1–B3) or 2.2 (A1, A2), which is consistent with the result of Weitz et al., where the fractal dimension of pyridine-induced gold nanoparticle aggregates was between 1.75 and 2.05 (±0.05) [20]. This suggests that final gold nanoparticle aggregates used in our study have a fractal structure with a mass fractal dimension of 2.1–2.2.

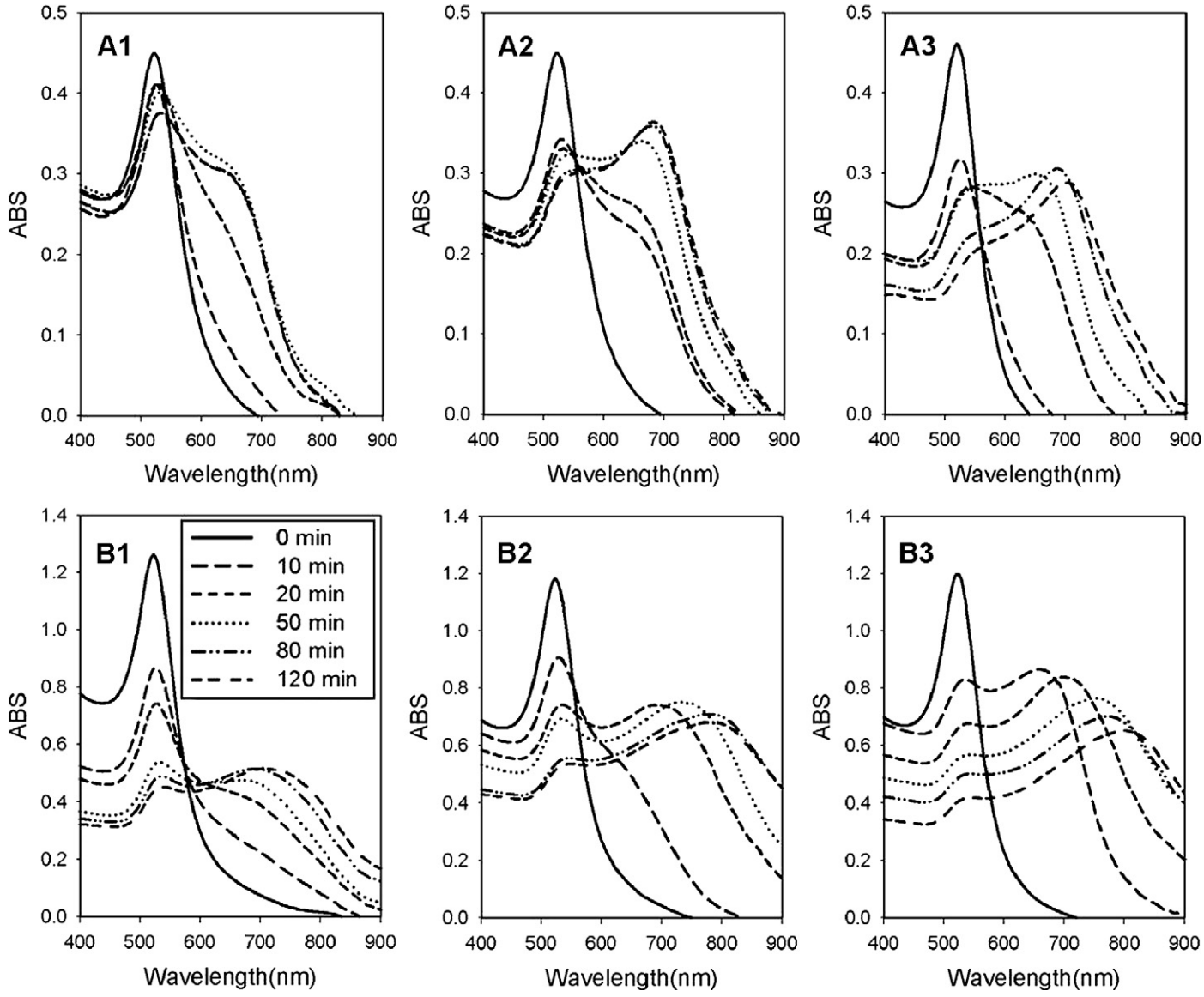

Fig. 2. Changes in the UV–vis absorption spectra after benzyl mercaptan addition.

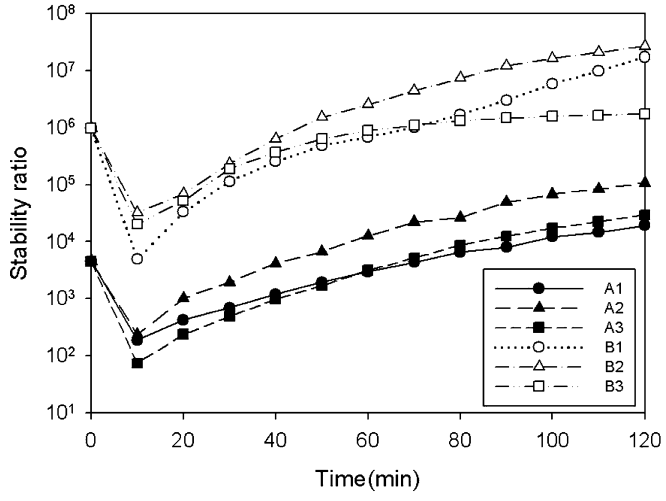

Fig. 3. Change in the stability ratio after benzyl mercaptan addition. The lines are drawn as a guide to the eye.

Using this value of fractal dimension, we estimate the mass ratio of aggregates to initial particles (i.e., total number of initial particles in an aggregate) as a function of time (Fig. 5). Appearance of the localized surface plasmon band is related to the corresponding color change of the gold nanoparticle suspension into blue, which determines the sensor response time. The shaded band in Fig. 5 is drawn over the different times at which the distinct localized surface plasmon band appears in the visible spectra of each sample. We find that the total number of initial particles in an aggregate that is responsible for the initial color change is close to 11 (11.5 ± 2.0). As indicated by the relatively narrow band, this number is consistent among all cases except A1, for which no color change was observed. This still remains to be tested in other systems involving gold nanoparticle aggregation, but the approach used in this paper can be applied to understand aggregation kinetics of other nanoparticle systems, and also to design and optimize colorimetric sensors based on gold nanoparticle aggregation.

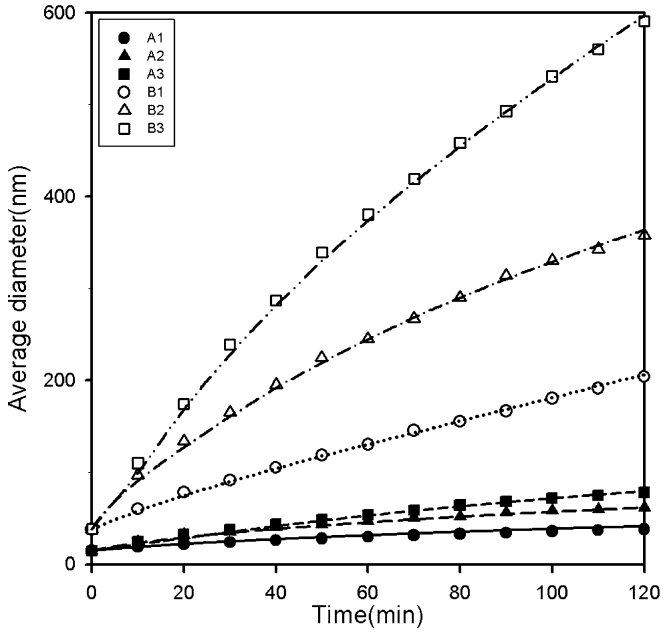

Fig. 4. The average diameter of samples versus time after benzyl mercaptan addition. The lines indicate the calculated values.

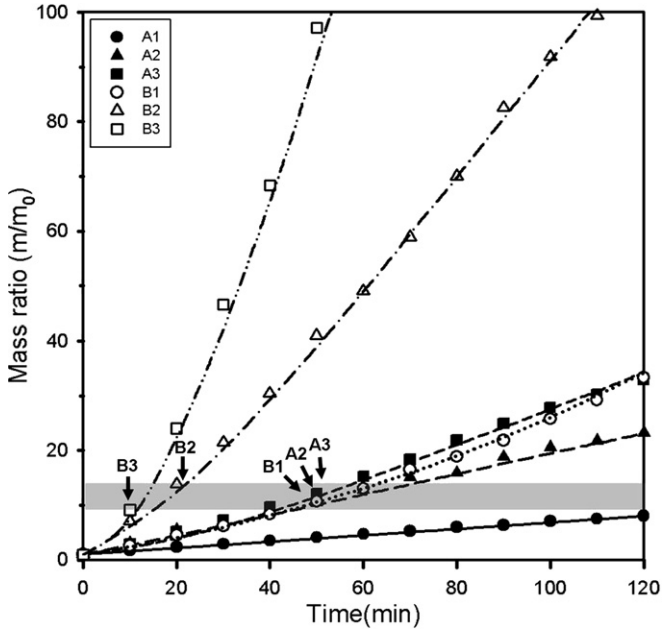

Fig. 5. The mass ratio of samples versus time after benzyl mercaptan addition. The lines indicate the calculated values, and the arrows indicate the time at which the distinct localized surface plasmon band appears in the UV–vis spectra. The shaded band is drawn over different times for the appearance of the localized surface plasmon bands of each sample.

4. Summary

We have performed a comprehensive kinetic study on gold nanoparticle aggregation using both experiments and mathematical modeling. We find that aggregation kinetics can be well described by the model based on classical DLVO theory. Our results indicate that aggregates have a fractal structure with a mass fractal dimension of 2.1–2.2. The initial color change of gold nanoparticle suspension appears to be caused by the aggregation of approximately 11 initial particles. To confirm these results, we are currently testing other target molecular systems that utilize gold nanoparticle aggregation. Our approach provides a general tool that enables prediction of the sensor response time and can be applied to the design of materials for various optical sensors.

Acknowledgments

K.L. thanks the KOSEF for financial support through Grant KOSEF 2007-8-1158 and the National Core Research Center for Nanomedical Technology (R15-2004-024-00000-0). S.W.J. acknowledges the financial support by the KOSEF (R01-2006-000-10017-0) and the Soongsil University Research Fun.

Appendix A. Nomenclature

A_H	Hamaker constant
a_i	radius of particle i
D_f	mass fractal dimension of the object
e	electronic charge
I	ionic strength
k	Boltzmann constant
m, m'	particle masses
N_A	Avogadro number
R	distance between the centers of two particles
s	the scaled distance between the centers of two particles ($s = 2R/(a_1 + a_2)$)
T	temperature
V_T	total interaction potential between two particles
v, v'	particle volumes
x	the closest distance between particle surfaces
ε	dielectric constant of the medium
κ	inverse of Debye length
μ	viscosity of medium
ψ_0	surface potential of the particle

References

[1] M. Faraday, Philos. Trans. 147 (1857) 145.
[2] M.K. Chow, C.F. Zukoski, J. Colloid Interface Sci. 165 (1994) 97.
[3] J. Turkevich, P.C. Stevenson, J. Hillier, Discuss. Faraday Soc. 11 (1951) 55.
[4] P. Alivisatos, Nat. Biotechnol. 22 (2004) 47.
[5] C. Weisbecker, M. Merritt, G. Whitesides, Langmuir 12 (1996) 3763.
[6] S. Peschel, G. Schmid, Angew. Chem. Int. Ed. Engl. 34 (1995) 1442.
[7] R. Elghanian, J. Storhoff, C. Mucic, R. Lestinger, C. Mirkin, Science 277 (1997) 1078.
[8] J. Storhoff, A. Lazarides, C. Mucic, C. Mirkin, R. Lestinger, G. Schatz, J. Am. Chem. Soc. 122 (2000) 4640.
[9] C. Mucic, J. Storhoff, C. Mirkin, R. Letsinger, J. Am. Chem. Soc. 120 (1998) 12674.
[10] U. Kreibig, M. Volmer, Optical Properties of Metal Clusters, Springer-Verlag, Berlin, 1995.
[11] I. Ruach-Nir, T.A. Bendikov, I. Doron-Mor, Z. Barkay, A. Vaskevich, I. Rubinstein, J. Am. Chem. Soc. 129 (2007) 84.
[12] M. Moskovits, B. Vlckova, J. Phys. Chem. B 109 (2005) 14755.
[13] R. Prasher, P.E. Phelan, P. Bhattacharya, Nano Lett. 6 (2006) 1529.

[14] N. Kallay, S.J. Zalac, J. Colloid Interface Sci. 253 (2002) 70.
[15] T. Laaksonen, P. Ahonen, C. Johans, K. Kontturi, ChemPhysChem 7 (2006) 2143.
[16] T. Kim, K. Lee, M. Gong, S.-W. Joo, Langmuir 21 (2005) 9524.
[17] R.J. Hunter, Foundations of Colloid Science, Clarendon Press, Oxford, 1992.
[18] E.J. Verwey, J.Th.G. Overbeek, Theory of the Stability of Lyophobic Colloids, Dover, New York, 1999.
[19] M. Smith, T. Matsoukas, Chem. Eng. Sci. 53 (1998) 1777.
[20] D.A. Weitz, J.S. Huang, M.Y. Lin, J. Sung, Phys. Rev. Lett. 54 (1985) 1416.
[21] P. Meakin, Ann. Rev. Phys. Chem. 39 (1988) 237.